# Charge-induced dipole vs. relativistically enhanced covalent interactions in Ar-tagged Au-Ag tetramers and pentamers

Shayeghi, A.; Schäfer, R.; Rayner, D. M.; Johnston, R. L.; Fielicke, A.

*DOI:*
10.1063/1.4923255

AIP | The Journal of Chemical Physics

# Charge-induced dipole vs. relativistically enhanced covalent interactions in Ar-tagged Au-Ag tetramers and pentamers

A. Shayeghi, R. Schäfer, D. M. Rayner, R. L. Johnston, and A. Fielicke

Citation: The Journal of Chemical Physics **143**, 024310 (2015); doi: 10.1063/1.4923255
View online: http://dx.doi.org/10.1063/1.4923255
View Table of Contents: http://scitation.aip.org/content/aip/journal/jcp/143/2?ver=pdfcov
Published by the AIP Publishing

# Charge-induced dipole vs. relativistically enhanced covalent interactions in Ar-tagged Au-Ag tetramers and pentamers

A. Shayeghi,[1,a)] R. Schäfer,[1] D. M. Rayner,[2] R. L. Johnston,[3] and A. Fielicke[4,a)]
[1]*Eduard-Zintl-Institut, Technische Universität Darmstadt, Alarich-Weiss-Straße 8, 64287 Darmstadt, Germany*
[2]*National Research Council of Canada, 100 Sussex Drive, Ottawa, Ontario K1A 0R6, Canada*
[3]*School of Chemistry, University of Birmingham, Edgbaston, Birmingham B15 2TT, United Kingdom*
[4]*Institut für Optik und Atomare Physik, Technische Universität Berlin, Hardenbergstrasse 36, 10623 Berlin, Germany*

(Received 11 May 2015; accepted 18 June 2015; published online 10 July 2015)

Vibrational spectra of $Au_nAg_m^+ \cdot Ar_k$ ($n + m = 4,5$; $k$ = 1-4) clusters are determined by far-infrared resonant multiple photon dissociation spectroscopy in the range $\tilde{\nu}$ = 100-250 $cm^{-1}$. The experimental spectra are assigned using density functional theory for geometries obtained by the Birmingham cluster genetic algorithm. Putative global minimum candidates of the Ar complexes are generated by adding Ar atoms to the $Au_nAg_m^+$ low energy isomers and subsequent local optimization. Differential Ar binding energies indicate exceptionally strong Au-Ar bonds in Au-rich clusters, leading to fundamental changes to the IR spectra. The stronger Ar binding is attributed to a relativistically enhanced covalent character of the Au-Ar bond, while in Au-rich species charge-induced dipole interactions overcompensate the relativistic affinity to Au. Moreover, not only the absolute composition but also the topologies are essential in the description of Ar binding to a certain cluster. © *2015 AIP Publishing LLC.* [http://dx.doi.org/10.1063/1.4923255]

## I. INTRODUCTION

Isolated clusters are important model systems in the study of physical and chemical properties of novel nanosized materials. Hereby, clusters of gold and silver have retained interest in recent decades,[1,2] though they have been studied since the dawn of nanoscience.[3] Their very interesting optical properties,[4–8] and chemical reactivities, have been intensively investigated up to particles containing several hundreds of atoms.[9,10] More recently, also mixed Au-Ag clusters have attracted great attention.[11,12] Controlling their properties by adjusting size, composition, topology, and chemical environment has opened a wide field of applications from nanophotonics,[13,14] and sensoring,[15] to catalysis,[16,17] and biodiagnostics.[18,19]

Their investigation at the atomic scale allows a bottom-up approach to underlying principles manifested in their unique properties. Following laser-induced fluorescence spectroscopy experiments on the AgAu dimer,[20] anionic $Ag_nAu_m^-$ ($2 \le n + m \le 4$) clusters have been examined by photoelectron spectroscopy, where Au is found to carry the negative charge and prefers lower coordination sites in the cluster.[21] Optical response calculations of mixed gold-silver clusters were investigated by time-dependent density functional theory (TDDFT) in several recent studies (and references within).[22–25]

Determining the geometries of such gas-phase clusters is the first step in studies of their intrinsic properties. Therefore, structural properties of cationic Au-Ag clusters up to five atoms $Ag_mAu_n^+$ ($m + n \le 5$) have been investigated employing ion mobility experiments.[26] The identified structures can be rationalized in terms of charge-transfer effects, which was also predicted theoretically for neutral and charged bimetallic $Ag_mAu_n$ ($3 \le m + n \le 5$) clusters.[27] Recently, also optical spectra of mixed $Ag_nAu_{4-n}^+$ ($n$ = 1-4) clusters have been measured by direct photodissociation spectroscopy, where competing structural motifs, including permutational isomers of given bimetallic geometries (homotops), have been discussed based on homo- and heterophilicity, electronegativity, atomic radii, and charge distribution effects.[28,29]

In this work, we present far-infrared multiple photon dissociation (FIR-MPD) spectra of $Au_nAg_m^+ \cdot Ar_k$ ($n + m = 4,5$; $k$ = 1-4) clusters in the range $\tilde{\nu}$ = 100-250 $cm^{-1}$, where the relatively weakly bound Ar atoms act as a probe for the absorption of IR photons. The experimental spectra are compared to calculated harmonic IR spectra for geometries obtained by the Birmingham Cluster Genetic Algorithm (BCGA) coupled with density functional theory (GADFT),[30,31] using the same level of theory as in calculations of the optical response for mixed tetramer cations.[29] Isomers from the global optimization are locally re-optimized including up to four Ar atoms for all possible configurations within a given bare isomer. Absolute and differential Ar binding energies are calculated in order to study the influence of the composition on the bond strength in the mixed cations.

The experimental approach of the messenger technique often assumes that the weakly bound ligands usually do not affect the electronic and geometric structures of their host clusters significantly. However, it has been previously shown, for neutral and small Au clusters tagged with krypton, that the noble-gas atom does not act as a mere messenger and has to be considered in the calculations as a complex.[32–34] For

a)Authors to whom correspondence should be addressed. Electronic addresses: fielicke@physik.tu-berlin.de and shayeghi@cluster.pc.chemie.tu-darmstadt.de

 

neutral Ag trimers it is found that noble-gas atoms lead to some band-shifts but do not perturb the vibrational spectrum significantly.[35] On the other hand, for noble-gas (Ng) complexes of the closed-shell coinage metal cations $M^+$ (M = Au, Ag, Cu), enhanced strengths of the $Au^+$–Ng bonds, as the Ng changes from He to Xe, was indicated by Pyykkö *et al.*[36,37] This concept was subject to numerous further studies,[38–45] and the stronger $Au^+$–Ng bonds are explained to be due to the relativistically increased electronegativity of Au, leading to an enhanced covalency of the Au-Ng interactions. The inclusion of Ar atoms is at the center of this study and will therefore be discussed in depth. The range of data allows an investigation of the cluster-Ng interaction, as depending on size, composition, topology and spin-state, as tetramer cations are open-shell molecules while the pentamers have a closed electronic shell. The influence of the messenger atom, depending on the proportion of Au, can be studied. Details on the interaction between the Ar ligands and the Au or Ag atoms within mixed trimer cations have been more thoroughly investigated and are discussed elsewhere.[46]

## II. EXPERIMENTAL AND COMPUTATIONAL DETAILS

Vibrational spectra are obtained by FIR-MPD spectroscopy using the messenger-atom technique, which has been described elsewhere.[47,48] Briefly, Ar-tagged Au-Ag cluster cations are formed by pulsed laser vaporization of a Au-Ag alloy target using a mixture of 0.25% Ar in He as the expansion gas. The clusters are thermalized to a temperature of 150 K while passing a cryogenic nozzle. After expansion into vacuum and passing a skimmer, the ion beam enters the extraction region of a reflectron time-of-flight mass spectrometer. An intense and tunable far-infrared pulse from the Free Electron Laser for Infrared eXperiments (FELIX)[49] irradiates the cluster beam in a counterpropagating fashion. A single pulse typically provides 20 mJ in a 10 $\mu$s long macropulse with a bandwidth of ≈1% of the full width at half-maximum (FWHM) of the central wavelength. If the IR radiation resonantly couples to a vibrational mode, multiple photons can be absorbed, which heats up the cluster and finally leads to a dissociation within the experimental time scale. The mass signal depletion due to this dissociation is monitored as a function of the FELIX wavelength. The resulting IR spectra are shown on a cross section scale (see Ref. 50 for details).

The configuration space for all considered clusters is searched using the GADFT global optimization approach. In the calculations, 11 electrons for each atom are treated explicitly and the remaining 36 and 68 core electrons for Ag and Au, respectively, are described by ultrasoft Rabe-Rappe-Kaxiras-Joannopoulos pseudopotentials.[51] For Au, a nonlinear correction and the Perdew-Burke-Ernzerhof (PBE)[52] exchange correlation (xc) functional is employed.

The lowest lying potential global minimum (GM) candidates are subsequently locally optimized using NWChem v6.3,[53] employing the def2-TZVPP basis set and the corresponding scalar relativistic small-core effective core potential (def2-ECP).[54] The long-range corrected xc functional, LC-$\omega$PBEh,[55,56] is used in order to recover the asymptotic $1/r$ behaviour. This has been shown to reliably reproduce vertical electronic excitation spectra,[28,29,56–60] while the higher amount of exact Hartree-Fock exchange at long-range has proven to be useful in describing the weaker MAr (M = Cu, Ag, Au) bonds in small Ar-tagged neutral clusters.[61] Relaxed geometries are further re-minimized by manually attaching Ar atoms to several positions at the cluster. The resulting optimized geometries are further used in harmonic frequency calculations to obtain IR linespectra, which are then convoluted with Gaussian functions with a FWHM of 5 $cm^{-1}$ for a better comparison to the experimental data (supplementary material available in Ref. 62).

The theoretical prediction of Ar binding energies by DFT calculations is generally uncertain since common xc functionals do not describe long-range dispersion interactions correctly. The development of DFT approaches that model dispersion interactions accurately is a research field with increasing interest in the literature.[63] Due to the very good agreement between the calculated harmonic IR spectra and the FIR-MPD experiments, but also to the agreement of the calculations with previous mass spectrometric studies from temperature-dependent Ar-tagging,[64] Ar binding energies from this study, using the LC-$\omega$PBEh functional, are expected to be reasonable and some useful trends can be derived from the following discussion. The calculated differential Ar binding energies for $Au_nAg_m^+ \cdot Ar_k \rightarrow Au_nAg_m^+ \cdot Ar_{k-1} + Ar$ in the calculations, for each size and composition, are only determined up to the number of Ar atoms actually observed in the experiments. Also, the calculated vibrational spectra of a given Au-Ag cluster composition are only compared to FIR-MPD spectra with the largest number of attached Ar atoms observed in the measurements.

## III. RESULTS AND DISCUSSION

### A. Tetramers

The bare tetramers considered in this study have been investigated by ion mobility measurements,[65] optical photodissociation spectroscopy,[28,64,66] and in DFT studies.[27] The three competing structural motifs in the open-shell molecules include the rhombus, the distorted tetrahedron, and the y-shape geometry. In the experiments, only $Au_4^+ \cdot Ar_k$ ($k$ = 0-3), $Au_3Ag^+ \cdot Ar_k$ ($k$ = 0-2), and $Au_2Ag_2^+ \cdot Ar_k$ ($k$ = 0-4) were found to have sufficient mass spectrometric abundance and are therefore the only systems considered in the following discussion.

#### 1. $Au_4^+$

The $Au_4^+ \cdot Ar_k$ ($k$ = 0-4) cluster has been intensively investigated by photodissociation spectroscopy combined with DFT (employing B3LYP) and RI-MP2 calculations using basis-sets of triple-$\zeta$ quality.[66] Here, only the rhombus shape is presented in Figure 1 since it is lowest in energy. The y-shape is not considered as it is 0.14 eV higher in energy and it appears not to contribute significantly to the IR spectrum, while from optical spectroscopy it was not possible to rule out a contribution.[28] The Ar binding energy for the first Ar atom obtained in this work is 0.21 eV for the short axis and

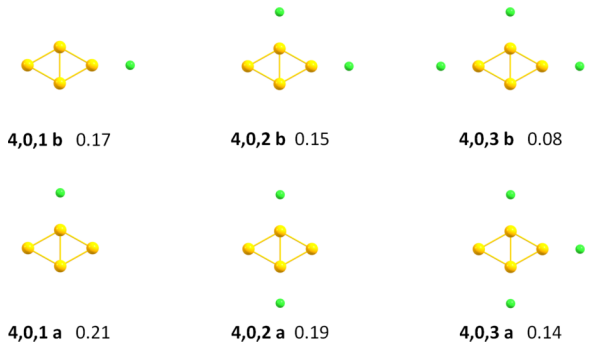


FIG. 1. Structures of $Au_4^+ \cdot Ar_k$ ($k$ = 1-3) clusters at the LC-$\omega$PBEh/def2-TZVPP level of theory. The bold numbers represent the $n,m,k$ in $Au_nAg_m^+ \cdot Ar_k$ followed by the differential Ar binding energies in eV. Out of plane isomers are less stable and therefore not shown here.

0.17 eV for the long axis and almost twice as large as from previous DFT calculations employing B3LYP. However, the RI-MP2 calculations agree well with the calculations reported here. The attachment of two more Ar atoms shows a decreasing trend in differential binding energies while obviously the short axis, carrying the larger partial charge, shows a stronger stabilization of Ar atoms in general.

The experimental FIR-MPD spectrum of the $Au_4^+ \cdot Ar_3$ cluster is presented in Fig. 2. Two isomers with three attached Ar atoms differently distributed are considered for the rhombus-shaped GM isomer. The calculated IR spectrum of isomer **4,0,3 a**, which is the most stable complex, shows very good agreement with the experimental mode at 106 $cm^{-1}$. The third Ar atom in isomer **4,0,3 b** is more weakly bound (0.08 eV), i.e., the complex is less stable and seems not to contribute to the measured spectrum. Its lowest frequency mode is slightly blue shifted (10 $cm^{-1}$) while the two weaker modes in the range 150-175 $cm^{-1}$ (present for both isomers) cannot be seen in the experimental spectrum, due to the low signal to noise ratio. Apparently, this approach is able to distinguish between the Ar species, though the signals of **4,0,3 b** are of lower intensity.

Interestingly, the harmonic IR spectrum of the bare $Au_4^+$ host cluster (dashed black line, scaled up by one order magnitude) differs significantly from the experimental FIR-MPD spectrum of its corresponding Ar-tagged species. It shows no significant transitions in the experimental range apart from a very low intensity mode below 150 $cm^{-1}$. Obviously, Ar atoms drastically influence the normal modes of the host cluster and do not act as mere messengers.

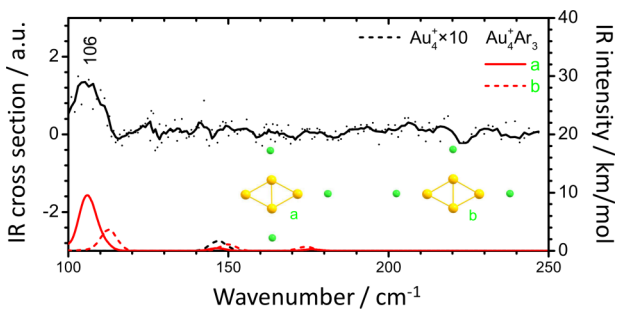


FIG. 2. FIR-MPD data points of the $Au_4^+ \cdot Ar_3$ cluster guided by a 5-pt. adjacent average compared to harmonic IR spectra at the LC-$\omega$PBEh/def2-TZVPP level of theory. Spectra of the respective bare isomers are additionally shown (dashed black line). Experimental peak positions are given in $cm^{-1}$ and are estimated to have an uncertainty of ±2 $cm^{-1}$.

## 2. $Au_3Ag^+$

The $Au_3Ag^+$ cluster is known to have a rhombus shaped GM structure, where the Ag atom occupies the higher coordinated short axis.[26,27,29] The next isomer is 0.18 eV higher in energy in the calculations and also rhombus shaped, with the Ag atom occupying the lower coordinated long axis. Ion mobility experiments and photodissociation spectroscopy clearly showed that no contribution of the higher lying rhombus has to be taken into account. Tagged species $Au_3Ag^+ \cdot Ar_k$ ($k$ = 1-2) within the GM rhombus geometry are shown in Figure 3, together with their differential binding energies. They are slightly smaller than in the pure $Au_4^+$ rhombus due to the single Ag dopant leading to a charge transfer from the Ag atom and resulting in weaker Ar binding to other sites. One could expect preferential Ar attachment at the short axis due to the large partial charge. However, Ar tagging on the Au atom, at the long axis, is preferred over the attachment at the short axis, although the long axis has the smaller partial charge, when compared to the short axis,[29] indicating the affinity for attachment to Au. This can also be seen in the doubly Ar-tagged species, where the attachment to both long sites **3,1,2 b** and both short sites **3,1,2 c** is almost degenerate. Overall, there is a competition between charge transfer effects depending on dopant sites and the increased strength of the Au-Ar bonds.

The experimental FIR-MPD spectrum of the $Au_3Ag^+ \cdot Ar_2$ cluster is presented in Fig. 4. For the $Au_3Ag^+ \cdot Ar_2$ cluster, the two species **3,1,2 a** and **3,1,2 b** have to be considered. The harmonic IR spectrum for **3,1,2 a**, which shows the strongest Ar binding of 0.14 eV, accurately describes the experimental spectrum. While isomer **3,1,2 b** may weakly contribute, **3,1,2 c** does not fit the data at all and is not discussed.

The harmonic IR spectrum of the bare $Au_3Ag^+$ host cluster (dashed black line) does not agree well with the experimental FIR-MPD spectrum of its corresponding Ar-tagged species. While the theoretical spectrum of $Au_4^+$ showed no significant transitions in the experimental range, the $Au_3Ag^+$ at least has the same vibrational signature, though the modes are shifted by about 20 $cm^{-1}$. This observation again shows a tremendous influence of the messenger atom, although the charge-transfer

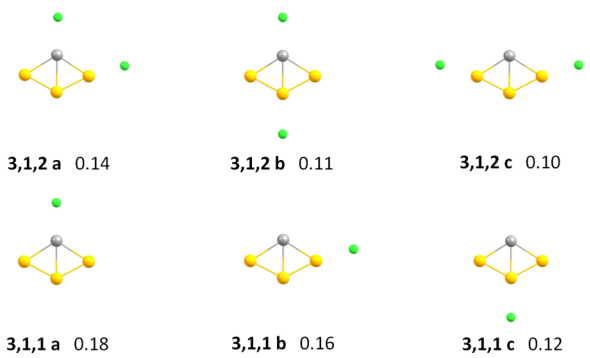


FIG. 3. Structures of $Au_3Ag^+ \cdot Ar_k$ ($k$ = 1-2) clusters at the LC-$\omega$PBEh/def2-TZVPP level of theory. For details, refer to Figure 1.

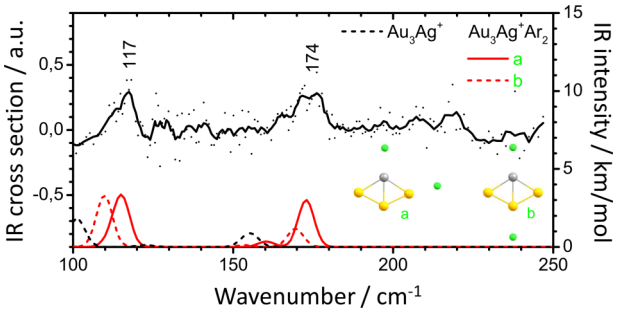


FIG. 4. FIR-MPD data points of the $Au_3Ag^+ \cdot Ar_2$ cluster guided by a 5-pt. adjacent average compared to harmonic IR spectra at the LC-$\omega$PBEh/def2-TZVPP level of theory. For details, refer to Figure 2.

from the Ag to the three Au atoms seems to reduce the Au-Ar bond strengths leading to a weaker influence of the Ar atom than in the case of pure $Au_4^+$.

### 3. $Au_2Ag_2^+$

The $Au_2Ag_2^+$ cluster is the most difficult tetramer due to several competing putative GM geometries,[26,27,29] and is discussed separately for the sake of clarity. The 50:50 mixture shows a very close competition within 0.2 eV of the GM, which is supposed to be the distorted tetrahedron at the present theory level. Their Ar species $Au_2Ag_2^+ \cdot Ar_k$ ($k$ = 1-4) are presented in Figure 5 in increasing relative isomer energy ordering from bottom up (bold numbers in eV). Two different rhombus structures, a distorted tetrahedron and several symmetric and non-symmetric y-shaped isomers, have been described previously. Ion mobility experiments supported by DFT calculations find the two rhombus shaped isomers to be almost degenerate and to best fit the experimental collision cross sections.[26] From these studies, the next higher lying y-shape (iso-2) and the quasitetrahedron (iso-1) can be ruled out.

Photodissociation spectroscopy experiments combined with DFT extended these investigations by optical spectra of the $Au_2Ag_2^+$ cluster compared to TDDFT calculations for all isomers within 0.2 eV (using the LC-$\omega$PBEh functional). Further, collision cross sections have been calculated including accurate Bader partial charges in ion mobility simulations.[29] The calculations confirm that the quasitetrahedron cannot fit the ion mobility experiments, although it is supposed to be lowest in energy. While the non-symmetric rhombus (iso-3) appears to be a slightly better fit to the experimental collision cross section than the symmetric (iso-4), taking Bader charges into account in simulations brings the y-shape structure closer into consideration. The optical spectra can potentially be explained by a sum of contributions from both rhombus shapes and/or the y-shape, while a contribution of the quasitetrahedron cannot be definitely excluded.

Of all isomers, the distorted tetrahedron shows the strongest Ar binding for the first two Ar atoms, although the differences are only small. The third and fourth Ar atoms are only weakly bound. This is in agreement with the site by site charge transfer calculations showing almost no partial charge on the Au atoms but very large partial charges on the Ag atoms in the quasitetrahedron.[29] It should be noted that there is a

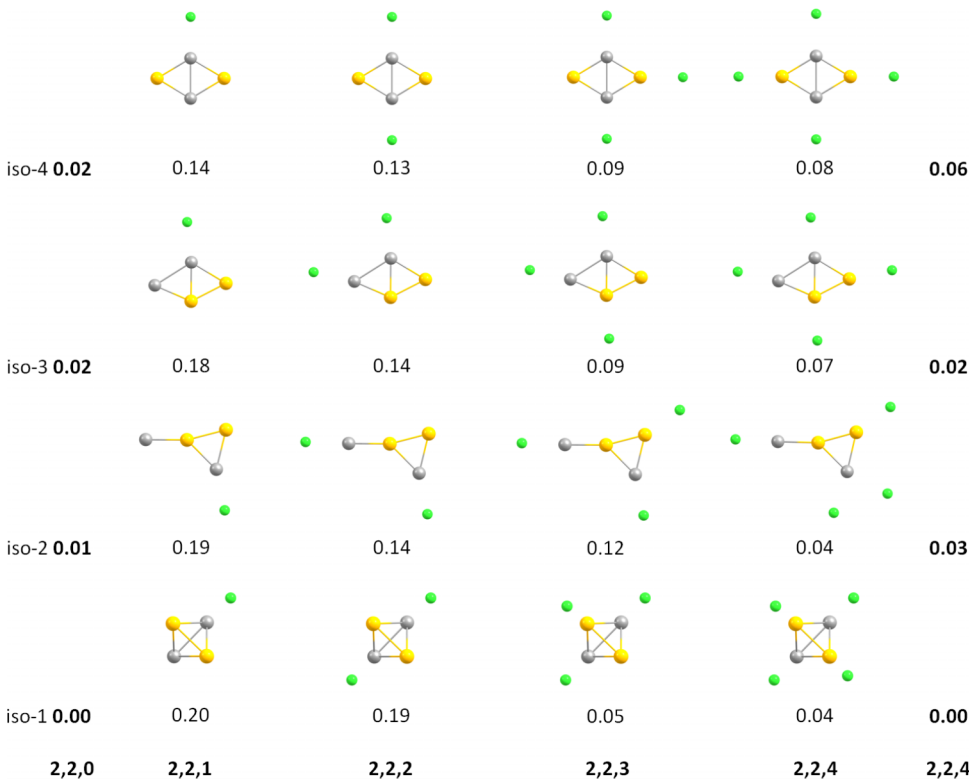


FIG. 5. Structures of $Au_2Ag_2^+ \cdot Ar_k$ ($k$ = 1-4) clusters at the LC-$\omega$PBEh/def2-TZVPP level of theory. The bold numbers represent the $n$,$m$,$k$ in $Au_nAg_m^+ \cdot Ar_k$. In the outer left and outer right column, relative energies of the bare isomers and the $Au_nAg_m^+ \cdot Ar_4$ clusters are presented in eV (bold), respectively. The differential Ar binding energies in eV are shown below the structures. Here, only the species with strongest binding energies within each structural isomer are presented for simplicity. The isomer energy ordering is slightly changed for 4 attached Ar atoms as can be seen in the outer right column.

minute reordering in isomer energies when considering the species tagged with four Ar atoms. Certainly, the differences are very small, but still may become relevant here. The quasitetrahedron, including four Ar atoms, remains the GM but the second lowest becomes the non-symmetrical rhombus shape (iso-3) with 0.02 eV to the GM while the y-shape (iso-2) lies slightly higher at 0.03 eV. The largest change appears for the symmetric rhombus (iso-4) with 0.06 eV to the GM. Thus, when up to four Ar atoms are attached, the energetic ordering can change in case of such a close competition between bare isomers.

Also in terms of vibrational spectra of the $Au_2Ag_2^+$ cluster, an assignment remains somehow inconclusive, as shown in Figure 6. Here, all low lying isomers, including four Ar atoms, are considered. While the first three isomers can potentially explain the FIR-MPD spectrum, iso-4 is the odd one out which cannot solely describe the experimental situation. However, the y-shape isomer (iso-2) does not agree well since it neither shows appropriate intensities nor fits all experimental transitions. Moreover, the vibrational mode at 122 $cm^{-1}$ does not appear in the experiment. The quasitetrahedron (iso-1) shows a better agreement in terms of the intensities of the linespectra but the broad experimental mode at 109 $cm^{-1}$ is also not well described. Though, from ion mobility experiments, the distorted tetrahedron can be excluded as potential GM structure. Therefore, the rhombus shaped iso-3 fits the ion mobility and FIR-MPD experiments best and including results from optical spectroscopy, other isomers (in particular iso-4), are expected to only weakly contribute to the experimental observations. However, a definite structural assignment for this composition may not be possible and it is not even clear if either several isomers contribute in the experiments or if the representation of static isomers is eventually not appropriate.

The calculated harmonic IR spectra of the bare $Au_2Ag_2^+$ isomers show an interesting dependence on the geometry regarding their agreement with IR spectra of their corresponding species tagged with four Ar atoms. For the tetrahedron (iso-1), similar intensities for all three transitions are found but the latter two are red-shifted by 10 $cm^{-1}$. The situation is worse in the following iso-2, while for iso-3 the IR spectrum of the bare cluster and its Ar-tagged species do not agree at all. In case of iso-4, the agreement between the noble-gas tagged and the bare cluster is much better. Interestingly, the species with larger Au-Au bond length (286 pm in iso-1 and no bond in iso-4) seem to behave like a Au-rich cluster, while species with short Au-Au distances (261 pm in iso-2 and 264 pm in iso-3) behave like Au-rich clusters.

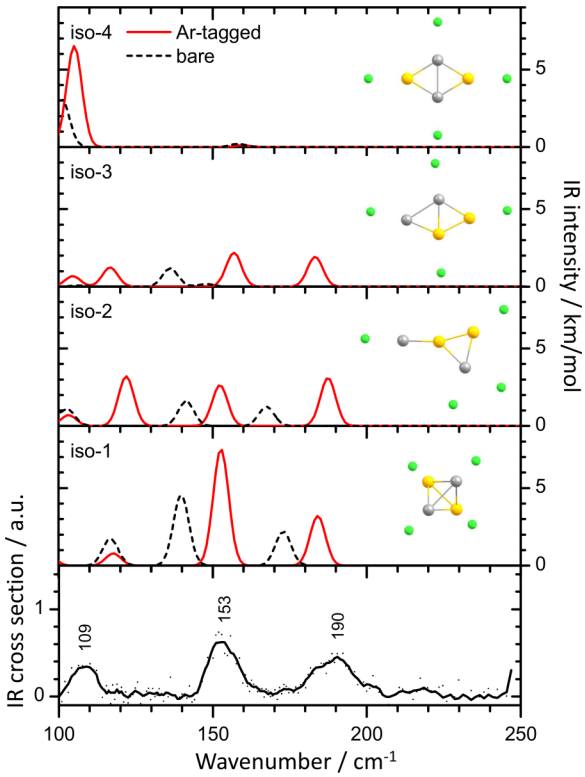


FIG. 6. FIR-MPD data points of $Au_2Ag_2^+ \cdot Ar_4$ clusters with a 5-pt. adjacent average as a guide to the eye compared to harmonic IR spectra at the LC-$\omega$PBEh/def2-TZVPP level of theory. For details, refer to Figure 2.

## B. Pentamers

The bare mixed pentamers are known from former ion mobility,[26] and reactivity studies,[67] supported by DFT studies.[27] Under the experimental conditions only $Au_5^+ \cdot Ar_k$ ($k$ = 0-4), $Au_4Ag^+ \cdot Ar_k$ ($k$ = 0-3), $Au_3Ag_2^+ \cdot Ar_k$ ($k$ = 0-2), and $Au_2Ag_3^+ \cdot Ar_k$ ($k$ = 0-1) were observed and are therefore the only pentamers discussed. The competing structural motifs in the closed–shell clusters mainly consist of planar and bow-tie geometries. Here, the interactions between the closed-shell pentamers and Ar atoms are expected to be similar to the $Au^+$–Ng closed-shell interactions,[36] as depending on charge distributions within compositions and their dopant sites.

### 1. $Au_5^+$

The $Au_5^+$ cluster is known to have a 2D planar bow-tie GM structure with $D_{2h}$ symmetry and a higher lying (0.03 eV) twisted 3D structure ($D_{2D}$), which appears to be a transition state with a very low imaginary frequency in both the calculations presented here and in previous studies.[26] The next higher lying isomer is a planar w-shape geometry at the BP86 level, which is not stable with LC-$\omega$PBEh. This isomer is followed by an edge capped tetrahedron 0.61 eV higher in energy. Therefore, only the bow-tie structure is discussed and its Ar species are presented in Figure 7. The differential binding energies for the successive Ar attachment to the GM show a decreasing trend and are in good agreement with experimental values.[64] In the case of the doubly Ar-tagged species, as expected from sterical aspects, the all-trans isomer **5,0,2** is the most stable and

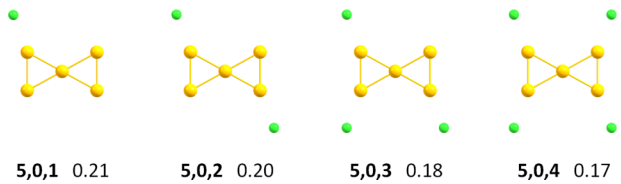


FIG. 7. Structures of the $Au_5^+ \cdot Ar_k$ ($k$ = 1-4) clusters at the LC-$\omega$PBEh/def2-TZVPP level of theory. For details, refer to Figure 1.

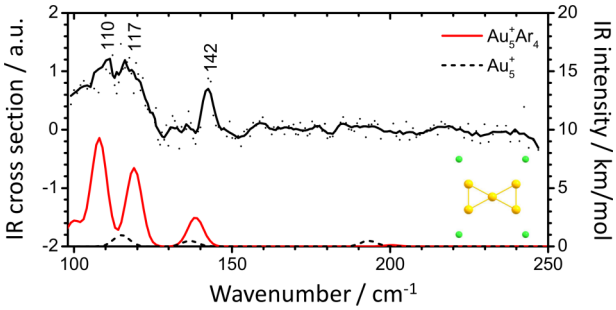


FIG. 8. FIR-MPD data points of the $Au_5^+ \cdot Ar_3$ cluster guided by a 5-pt. adjacent average compared to harmonic IR spectra at the LC-$\omega$ PBEh/def2-TZVPP level of theory. For details, refer to Figure 2.

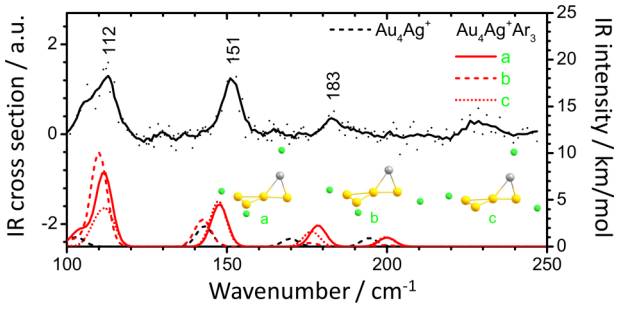


FIG. 10. FIR-MPD data points of the $Au_4Ag^+ \cdot Ar_2$ cluster guided by a 5-pt. adjacent average compared to harmonic IR spectra at the LC-$\omega$PBEh/def2-TZVPP level of theory. For details, refer to Figure 2.

therefore the only doubly tagged $Au_5^+ \cdot Ar_2$ cluster presented. There are also several out of plane Ar-tagged isomers, which are higher in energy and also not discussed.

The harmonic IR spectrum of the $Au_5^+ \cdot Ar_4$ cluster **5,0,4** in Fig. 8 accurately matches the experimental observations in terms of intensities and frequencies. Only the experimental transition at 142 $cm^{-1}$ is described to be slightly red-shifted in the calculations by about 5 $cm^{-1}$. Still there is a very good agreement between theory and experiment showing that the 2D planar bow-tie structure certainly is the GM, also when four Ar atoms are attached to the cluster.

The harmonic IR spectrum of the bare $Au_5^+$ host cluster (dashed black line) does not agree at all with the experimental FIR-MPD spectrum. Certainly, the Ar atoms have a pronounced influence on the spectra indicating a remarkable change in the electronic structure of the host cluster.

### 2. $Au_4Ag^+$

The $Au_4Ag^+$ cluster is known to have a 3D twisted bow-tie structure where the Ag atom occupies a corner instead of the higher coordinated central position.[26] The next higher lying isomer, 0.38 eV above the GM, is an edge capped tetrahedron where the Ag atom has an edge position, which was not stable in the optimizations. However, a planar transition state is additionally found with a very low imaginary frequency, which

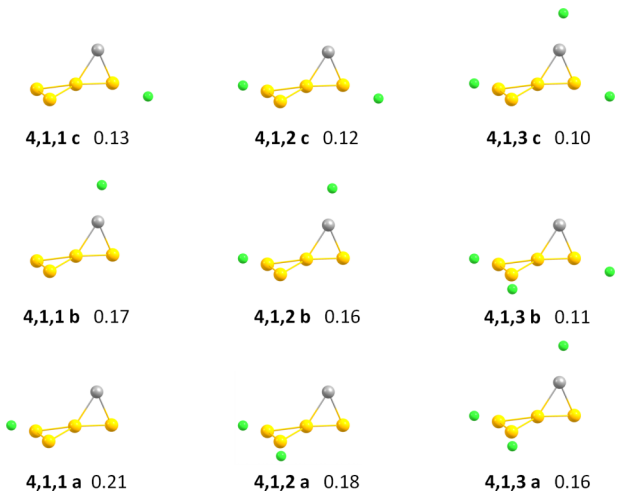


FIG. 9. Structures of the $Au_4Ag^+ \cdot Ar_k$ ($k$ = 1-3) cluster at the LC-$\omega$PBEh/def2-TZVPP level of theory. For details, refer to Figure 1.

is a planar bow-tie isomer of the GM with a relative energy of 0.03 eV. The next higher lying structure (0.38 eV) is again a 3D twisted bow-tie structure where now the Ag atom is centered. Thus, only the putative GM with $C_s$ symmetry is considered in Figure 9. In this Au-rich composition, the differential binding energy has the largest value for an attachment to the $Au_3$ triangle instead of the Ag atom, as can be seen for **4,1,1 a**. This behavior continues for the attachment of two Ar atoms, where the triangle is first tagged with Ar in **4,1,2 a**. The third Ar atom is then attached to the Ag atom, as a strong charge transfer from the Ag to the Au atom causes the charge-induced dipole interactions with the Ag atom to overcompensate the affinity of binding to Au. Hence, it is not surprising that **4,1,3 a** is the most stabilized complex while **4,1,3 b** and **4,1,3 c** are almost degenerate.

The $Au_4Ag^+ \cdot Ar_3$ spectra in Fig. 10 clearly give a better agreement for the species where Ar atoms are attached to the Au triangle. Isomer **4,1,3 b**, which has the second largest differential Ar binding energy, seems not to appear in the experiment while isomers **4,1,3 a** and **4,1,3 c** fit very well. The FIR-MPD spectrum also shows a broad feature at 230 $cm^{-1}$, which does not show up in any of the calculations and is possibly a combination mode. In conclusion, it can be asserted that the 3D twisted bow-tie structure is identified as structure of the $Au_4Ag^+ \cdot Ar_3$ cluster.

The calculation for the bare $Au_4Ag^+$ cluster (dashed black line) does somewhat better agree as in case of $Au_5^+$. Nevertheless, in spite of the single Ag dopant the Ar atoms have to be considered to achieve agreement with the experimental spectrum.

### 3. $Au_3Ag_2^+$

The $Au_3Ag_2^+$ cluster is also known to have a 3D twisted bow-tie GM structure, where Ag atoms occupy two corners, one in each triangle. The next higher lying isomer is a 3D twisted bow-tie structure as well, where the Ag atoms are *cis*-located.[26] This isomer lies 0.33 eV higher in energy at the present theory level and is therefore not considered. The structures and Ar binding energies of the $Au_3Ag_2^+ \cdot Ar_k$ ($k$ = 1-2) GM clusters are presented in Figure 11. The Ar atoms likely attach to the Ag positions since the attachment to Au leads to weakly bound complexes, as can be seen in the differential binding energy of 0.05 eV for **3,2,2 d**. Here, the increased amount of Ag changes the Ar binding and Ag atoms are more likely tagged.

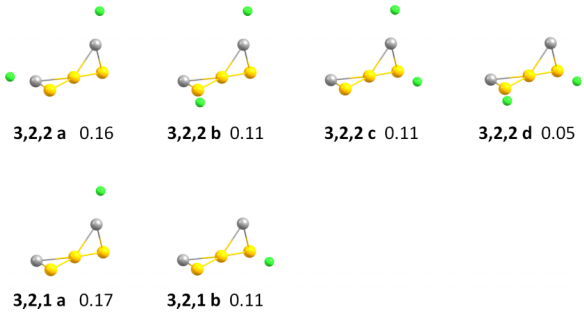


FIG. 11. Structures of the $Au_3Ag_2^+ \cdot Ar_k$ ($k = 1$-2) cluster at the LC-$\omega$PBEh/def2-TZVPP level of theory. For details, refer to Figure 1.

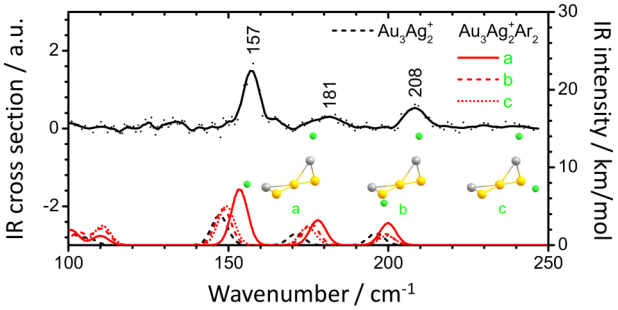


FIG. 12. FIR-MPD data points of the $Au_3Ag_2^+ \cdot Ar_2$ cluster guided by a 5-pt. adjacent average compared to harmonic IR spectra at the LC-$\omega$PBEh/def2-TZVPP level of theory. For details, refer to Figure 2.

The higher amount of Ag leads to strong charge-transfer from Ag to Au atoms and thus to a reduced charge-transfer from Ng atoms to Au, which ultimately causes a preferred coverage of the partially positively charged Ag atoms, overcompensating the binding strength to Au sites.

The harmonic IR spectrum for the $Au_3Ag_2^+ \cdot Ar_2$ cluster in Fig. 12 shows the best agreement for species where only Ag atoms are tagged with Ar (**3,2,2 a**). Results are, however, also shown for the other species where both Ag and Au atoms are tagged with Ar (**3,2,2 b** and **3,2,2 c**). While the calculations for **3,2,2 a** match the experimental findings, **3,2,2 d**, with the lowest differential binding energy of 0.05 eV, does not fit at all. Given the very good agreement with the experimental FIR-MPD spectrum obtained for the more stable Ar complexes, confidently the 3D twisted bow-tie structure is the GM of the $Au_3Ag_2^+ \cdot Ar_2$ cluster.

The calculations for the bare $Au_3Ag_2^+$ cluster (dashed black line) qualitatively agree with the FIR-MPD spectrum. The increased amount of Ag atoms and the resulting significant charge transfer to the Au atoms lead to a smaller effect on the cluster by the Ar atoms, but their inclusion still leads to better agreement in terms of frequencies and intensities.

### 4. $Au_2Ag_3^+$

The $Au_2Ag_3^+$ cluster is an interesting case as ion mobility experiments show two nearly degenerate isomers being present in the molecular beam from two different arrival time distributions.[26] The lowest lying isomer is a trigonal bipyramid where the Ag atoms form the triangle in a plane capped by Au atoms. The second lowest isomer, which is 0.07 eV higher in energy, is a 3D twisted bow-tie structure with a Au atom in the center. The next lying structure (a bow-tie geometry with a Ag atom in the center) is 0.26 eV higher in energy and therefore not considered. The corresponding $Au_2Ag_3^+ \cdot Ar$ clusters are presented in Figure 13. A single Ar atom attached to iso-1 is bound to the Ag triangle (**2,3,1 a**) while the attachment to Au (**2,3,1 b**) shows a very low binding energy of 0.04 eV. A similar situation can be seen in the bow-tie structure iso-2 where Ag atoms are more likely tagged with Ar. Again, the now dominant amount of Ag leads to a strong charge-transfer from Ag to Au atoms, causing a preferred coverage of the Ag atom in direct neighborhood to the Au atom, as it has the largest partial charge due to the larger electronegativity of Au.

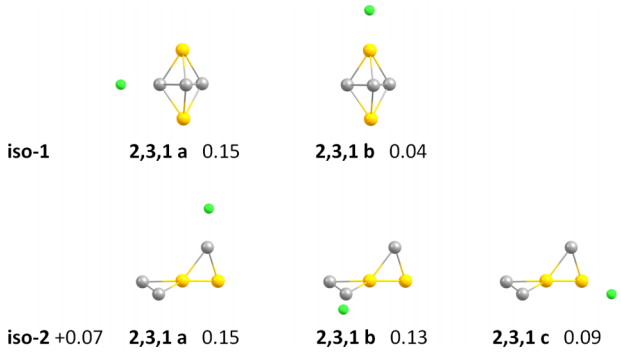


FIG. 13. Structures of the $Au_2Ag_3^+ \cdot$ Ar cluster at the LC-$\omega$PBEh/def2-TZVPP level of theory. For details, refer to Figure 1.

One may also notice that, beginning from the Au-rich compositions down to this silver-rich composition, there is a tendency for a decreasing number of attached Ar atoms in the experiments. This preference of a more likely attachment to Au-rich species points to the higher stability of Ar-tagged clusters with a higher amount of Au.

The $Au_2Ag_3^+$ spectra are shown in Fig. 14. Since it is known from ion mobility studies that both lowest lying isomers, the trigonal bipyramid (iso-1) and the 3D twisted bow-tie structure (iso-2), co-exist they may also contribute to the experiments here and have to be considered. If one assumes that in case of iso-1 only **2,3,1 a** and in case of iso-2 only **2,3,1 a** and **2,3,1 b** are present in the molecular beam (where only Ag atoms are tagged with Ar), the signature of the FIR-MPD spectrum can be interpreted as a sum of these three contributions, although the signal to noise ratio is not very satisfactory. Therefore, one can conclude that also in FIR-MPD

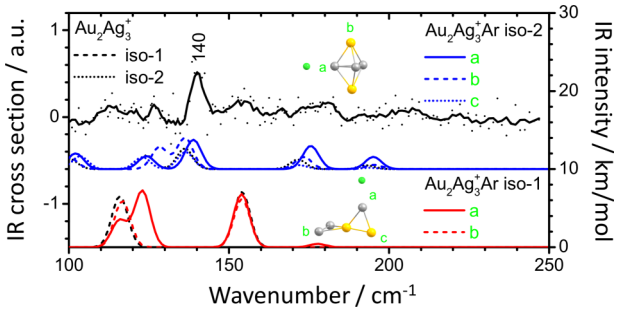


FIG. 14. FIR-MPD data points of the $Au_2Ag_3^+ \cdot Ar$ cluster guided by a 5-pt. adjacent average compared to harmonic IR spectra at the LC-$\omega$PBEh/def2-TZVPP level of theory. For details, refer to Figure 2.

experiments performed on the Ar complexes, both isomers are probably present in the molecular beam asserting earlier predictions from ion mobility experiments.

The IR spectra of the bare isomers of $Au_2Ag_3^+$ (dashed and dotted black lines for iso-1 and iso-2, respectively) agree well with calculations for the Ar-tagged clusters. Notably, the harmonic IR spectra of these bare clusters best agree with spectra of Ar-tagged isomers, where Ar atoms are bound to Au atoms. These are expected to be less stable in these silver-rich systems, as the Au atoms experience strong charge-transfer from the Ag atoms resulting in weak interactions with their positions.

## IV. CONCLUSIONS

Vibrational spectra of $Au_nAg_m^+ \cdot Ar_k$ ($n + m = 4,5$; $k = 1\text{-}4$) clusters have been measured using the Ar-messenger FIR-MPD method. Harmonic IR spectra from DFT calculations using the LC-$\omega$PBEh functional give very reasonable results consistent with the experimental spectra and with several previous combined experimental and theoretical studies. Overall, structural assignment has been carried out by a comparison of experimental and theoretical vibrational modes. The considered structures, known from previous ion mobility investigations and photodissociation spectroscopy studies, could be found in the experiments. Generally, clusters with high Ar coverage have been investigated but the metal cores of the GM structures still remain the same as for the bare clusters. Although the total Ar binding energies are significant, they do not differ much between the various (bare) cluster isomers with the result that Ar attachment is not remarkably changing the energetic order, despite the competition being very close, which is a relevant finding. Further, Ar binding energies of several Ar-tagged clusters of different size and composition could be derived indicating strong binding energies in the Au-rich species. Furthermore, it has been shown that Au-rich clusters are only weakly affected by Ar atoms and behave like the unperturbed clusters being surrounded by messenger atoms. In case of the Au-rich compositions, Ar atoms are involved in the transitions and the tagged clusters show molecule-like vibrational modes. These findings have been thoroughly discussed elsewhere in case of mixed trimeric Au-Ag clusters,[46] where the effects have been interpreted in terms of covalent interactions, charge transfer effects, and ion-induced dipole interactions. Presumably, in Au-rich clusters the covalent character of the bonds to Ar atoms is enhanced due to the high electronegativity of Au, reflecting relativistic effects, while in Au-rich clusters charge transfer from Ag to Au atoms leads to a stronger influence of ion-induced dipole interactions dominating the attachment.

## ACKNOWLEDGMENTS

We gratefully acknowledge the support of the Stichting voor Fundamenteel Onderzoek der Materie (FOM) for providing beam time on FELIX, and the FELIX staff for their skilful assistance, in particular Dr. B. Redlich and Dr. A. F. G. van der Meer. This work is supported by the Fritz-Haber Institute of the Max-Planck Society, the Cluster of Excellence: Unifying Concepts in Catalysis coordinated by the Technical University Berlin and funded by the Deutsche Forschungsgemeinschaft (DFG). We acknowledge financial support by the DFG (Grant Nos. SCHA 885/10-2 and FI 893/3) and the Merck'sche Gesellschaft für Kunst und Wissenschaft e. V.

The calculations reported here are performed on the following HPC facilities: The University of Birmingham BlueBEAR facility;[68] the MidPlus Regional Centre of Excellence for Computational Science, Engineering and Mathematics, funded under EPSRC Grant No. EP/K000128/1; and via our membership of the UK's HPC Materials Chemistry Consortium, which is funded by EPSRC (Grant No. EP/L000202). This work made use of the facilities of ARCHER, the UK's national high-performance computing service, which is funded by the Office of Science and Technology through EPSRC's High End Computing Programme. Special thanks are extended to Michael C. Böhm, Michael Langeloth, and Marc Jäger (Darmstadt).

[1]P. Schwerdtfeger, Angew. Chem., Int. Ed. **42**, 1892 (2003).
[2]R. Ferrando, J. Jellinek, and R. L. Johnston, Chem. Rev. **108**, 845 (2008).
[3]M. Faraday, Philos. Trans. R. Soc. London **147**, 145 (1857).
[4]S. Fedrigo, W. Harbich, and J. Buttet, J . Chem. Phys. **99**, 5712 (1993).
[5]B. A. Collings, K. Athanassenas, D. Lacombe, D. M. Rayner, and P. A. Hackett, J. Chem. Phys. **101**, 3506 (1994).
[6]M. M. Alvarez, J. T. Khoury, T. G. Schaaff, M. N. Shafigullin, I. Vezmar, and R. L. Whetten, J. Phys. Chem. B **101**, 3706 (1997).
[7]M. Harb, F. Rabilloud, D. Simon, A. Rydlo, S. Lecoultre, F. Conus, V. Rodrigues, and C. Félix, J . Chem. Phys. **129**, 194108 (2008).
[8]A. Terasaki, S. Minemoto, M. Iseda, and T. Kondow, Eur. Phys. J. D **9**, 163 (1999).
[9]M. Haruta, T. Kobayashi, H. Sano, and N. Yamada, Chem. Lett. **16**, 405 (1987).
[10]L. M. Molina, S. Lee, K. Sell, G. Barcaro, A. Fortunelli, B. Lee, S. Seifert, R. E. Winans, J. W. Elam, and M. J. Pellin, Catal. Today **160**, 116 (2011).
[11]D. R. Kauffman, D. Alfonso, C. Matranga, H. Qian, and R. Jin, J . Phys. Chem. C **117**, 7914 (2013).
[12]C. Kumara, C. Aikens, and A. Dass, J. Phys. Chem. Lett. **5**, 461 (2014).
[13]J. K. Gansel, M. Thiel, M. S. Rill, M. Decker, K. Bade, V. Saile, G. von Freymann, S. Linden, and M. Wegener, Science **325**, 1513 (2009).
[14]S. Wang, X. Meng, A. Das, T. Li, Y. Song, T. Cao, X. Zhu, M. Zhu, and R. Jin, Angew. Chem., Int. Ed. Engl. **53**, 2376 (2014).
[15]M. Käll, Nat. Mater. **11**, 570 (2012).
[16]M. V. Petri, R. A. Ando, and P. H. Camargo, Chem. Phys. Lett. **531**, 188 (2012).
[17]T. J. A. Slater, A. Macedo, S. L. M. Schroeder, M. G. Burke, P. O'Brien, P. H. C. Camargo, and S. J. Haigh, Nano Lett. **14**, 1921 (2014).
[18]N. L. Rosi and C. A. Mirkin, Chem. Rev. **105**, 1547 (2005).
[19]M. Larguinho and P. V. Baptista, J. Proteomics **75**, 2811 (2012).
[20]J. C. Fabbi, J. D. Langenberg, Q. D. Costello, M. D. Morse, and L. Karlsson, J. Chem. Phys. **115**, 7543 (2001).
[21]Y. Negishi, Y. Nakamura, A. Nakajima, and K. Kaya, J. Chem. Phys. **115**, 3657 (2001).
[22]G.-F. Zhao, J.-M. Sun, and Z. Zeng, Chem. Phys. **342**, 267 (2007).
[23]X.-D. Zhang, M.-L. Guo, D. Wu, P.-X. Liu, Y.-M. Sun, L.-A. Zhang, Y. She, Q.-F. Liu, and F.-Y. Fan, Int. J. Mol. Sci. **12**, 2972 (2011).
[24]X. López-Lozano, C. Mottet, and H.-C. Weissker, J . Phys. Chem. C **117**, 3062 (2013).
[25]H.-Ch. Weissker, R. L. Whetten, and X. López-Lozano, Phys. Chem. Chem. Phys. **16**, 12495 (2014).
[26]P. Weis, O. Welz, E. Vollmer, and M. M. Kappes, J. Chem. Phys. **120**, 677 (2004).
[27]V. Bonačić-Koutecký, J. Burda, R. Mitrić, M. Ge, G. Zampella, and P. Fantucci, J. Chem. Phys. **117**, 3120 (2002).
[28]A. Shayeghi, R. L. Johnston, and R. Schäfer, Phys. Chem. Chem. Phys. **15**, 19715 (2013).
[29]A. Shayeghi, C. J. Heard, R. L. Johnston, and R. Schäfer, J. Chem. Phys. **140**, 054312 (2014).
[30]R. L. Johnston, Dalton Trans. **2003**, 4193.

[31]S. Heiles, A. J. Logsdail, R. Schäfer, and R. L. Johnston, Nanoscale **4**, 1109 (2012).
[32]L. M. Ghiringhelli, P. Gruene, J. T. Lyon, D. M. Rayner, G. Meijer, A. Fielicke, and M. Scheffler, New J. Phys. **15**, 083003 (2013).
[33]L. A. Mancera and D. M. Benoit, J. Phys. Chem. A **119**, 3075 (2015).
[34]L. M. Ghiringhelli and S. V. Levchenko, Inorg. Chem. Commun. **55**, 153 (2015).
[35]A. Fielicke, I. Rabin, and G. Meijer, J. Phys. Chem. A **110**, 8060 (2006).
[36]P. Pyykkö, J. Am. Chem. Soc. **117**, 2067 (1995).
[37]D. Schröder, H. Schwarz, J. Hrusak, and P. Pyykkö, Inorg. Chem. **37**, 624 (1998).
[38]J. P. Read and A. D. Buckingham, J. Am. Chem. Soc. **119**, 9010 (1997).
[39]R. Wesendrup, T. Hunt, and P. Schwerdtfeger, J. Chem. Phys. **112**, 9356 (2000).
[40]D. Bellert and W. H. Breckenridge, Chem. Rev. **102**, 1595 (2002).
[41]W. H. Breckenridge, V. L. Ayles, and T. G. Wright, J. Phys. Chem. A **112**, 4209 (2008).
[42]T. Zeng and M. Klobukowski, J. Phys. Chem. A **112**, 5236 (2008).
[43]L. Belpassi, I. Infante, F. Tarantelli, and L. Visscher, J. Am. Chem. Soc. **130**, 1048 (2008).
[44]P. Zhang, Y. Zhao, F. Hao, X. Song, G. Zhang, and Y. Wang, J. Mol. Struct.: THEOCHEM **899**, 111 (2009).
[45]Z. Jamshidi, K. Eskandari, and S. M. Azami, Int. J. Quantum Chem. **113**, 1981 (2013).
[46]A. Shayeghi, R. L. Johnston, D. M. Rayner, R. Schäfer, and A. Fielicke, "Messenger or modifier? The nature of argon bonds to mixed gold-silver trimers," Angew. Chem., Int. Ed. (in press).
[47]A. Fielicke, G. von Helden, and G. Meijer, Eur. Phys. J. D **34**, 83 (2005).
[48]A. Fielicke, A. Kirilyuk, C. Ratsch, J. Behler, M. Scheffler, G. von Helden, and G. Meijer, Phys. Rev. Lett. **93**, 023401 (2004).
[49]D. Oepts, A. F. G. van der Meer, and P. W. van Amersfoort, Infrared Phys. Technol. **36**, 297 (1995).
[50]P. Gruene, B. Butschke, J. T. Lyon, D. M. Rayner, and A. Fielicke, Z. Phys. Chem. **228**, 337 (2014).
[51]A. M. Rappe, K. M. Rabe, E. Kaxiras, and J. D. Joannopoulos, Phys. Rev. B **41**, 1227 (1990).
[52]J. Perdew, K. Burke, and M. Ernzerhof, Phys. Rev. Lett. **77**, 3865 (1996).
[53]M. Valiev, E. J. Bylaska, N. Govind, K. Kowalski, T. P. Straatsma, H. J. J. Van Dam, D. Wang, J. Nieplocha, E. Apra, T. L. Windus, and W. A. de Jong, Comput. Phys. Commun. **181**, 1477 (2010).
[54]F. Weigend and R. Ahlrichs, Phys. Chem. Chem. Phys. **7**, 3297 (2005).
[55]O. A. Vydrov and G. E. Scuseria, J. Chem. Phys. **125**, 234109 (2006).
[56]M. A. Rohrdanz, K. M. Martins, and J. M. Herbert, J. Chem. Phys. **130**, 054112 (2009).
[57]D. W. Silverstein and L. Jensen, J. Chem. Phys. **132**, 194302 (2010).
[58]J. V. Koppen, M. Hapka, M. M. Szcześniak, and G. Chalasinski, J. Chem. Phys. **137**, 114302 (2012).
[59]F. Rabilloud, J. Phys. Chem. A **117**, 4267 (2013).
[60]A. Shayeghi, R. L. Johnston, and R. Schäfer, J. Chem. Phys. **141**, 181104 (2014).
[61]Z. Jamshidi, M. F. Far, and A. Maghari, J. Phys. Chem. A **116**, 12510 (2012).
[62]See supplementary material at http://dx.doi.org/10.1063/1.4923255 for atomic coordinates and harmonic IR linespectra of the considered isomers.
[63]S. Grimme, Wiley Interdiscip. Rev.: Comput. Mol. Sci. **1**, 211 (2011).
[64]S. M. Lang, P. Claes, N. T. Cuong, M. T. Nguyen, P. Lievens, and E. Janssens, J. Chem. Phys. **135**, 224305 (2011).
[65]P. Weis, Int. J. Mass Spectrom. **245**, 1 (2005).
[66]A. Schweizer, J. M. Weber, S. Gilb, H. Schneider, D. Schooss, and M. M. Kappes, J. Chem. Phys. **119**, 3699 (2003).
[67]M. Neumaier, F. Weigend, O. Hampe, and M. M. Kappes, J. Chem. Phys. **125**, 104308 (2006).
[68]See http://www.bear.bham.ac.uk/bluebear for a description of the BlueBEAR HPC facility.